Inorganic Chemistry

Article

pubs.acs.org/IC

Investigation on NMR Relaxivity of Nano-Sized Cyano-Bridged Coordination Polymers

Marine Perrier,[†] Samir Kenouche,[‡] Jêrôme Long,[†] Kalaivani Thangavel,[§] Joulia Larionova,*[,†] Christophe Goze-Bac,[‡] Alessandro Lascialfari,[§,∥] Manuel Mariani,[⊥] Nathalie Baril,[#] Christian Guérin,[†] Bruno Donnadieu,[¶] Alexander Trifonov,[□] and Yannick Guari[†]

[†]Institut Charles Gerhardt Montpellier, UMR 5253 CNRS-UM2-ENSCM-UM1, Chimie Moléculaire et Organisation du Solide, Université Montpellier II, Place E. Bataillon, 34095 Montpellier cedex 5, France

[‡]Laboratoire Charles Coulomb (L2C) BioNanoNMRI UMR 5221, Université Montpellier II, Montpelier, France

[§]Dipartimento di Fisica and INSTM, Università degli studi di Milano, I-201334 Milano, Italy

[∥]Centro S3, CNR-Istituto di Nanoscienze, I-41125 Modena, Italy

[⊥]Dipartimento di Fisica e Astronomia, Università degli studi di Bologna, 40126 Bologna, Italy

[#]Fédération de recherche 3C, FR 3512, CNRS-Aix-Marseille Université, 3 place Victor Hugo, 13331 Marseille cedex 3, France

[¶]Fédaration de Recherche Chimie Balard- FR3105, Université Montpellier II, Place E. Bataillon, 34095 Montpellier cedex 5, France

[□]G. A. Razuvaev Institute of Organometallic Chemistry of the Russian Academy of Science, Tropinina 49, GSP-44S, 603950, Nizhny Novgorod, Russia

Supporting Information

ABSTRACT: We present the first comparative investigation of the Nuclear Magnetic Resonance (NMR) relaxivity of a series of nanosized cyano-bridged coordination networks stabilized in aqueous solution. These $Ln^{3+}/[Fe(CN)_6]^{3-}$ (Ln = Gd, Tb, Y) and $M^{2+}/[Fe(CN)_6]^{3-}$ (M = Ni, Cu, Fe) nanoparticles with sizes ranging from 1.4 to 5.5 nm are stabilized by polyethylene glycols (MW = 400 or 1000), polyethylene glycol functionalized with amine groups (MW = 1500), or by N-acetyl-D-glucosamine. The evaluation of NMR relaxivity allowed estimation of the Magnetic Resonance Imaging (MRI) contrast efficiency of our systems. The results demonstrate that $Gd^{3+}/[Fe(CN)_6]^{3-}$ nanoparticles have r_{1p} and r_{2p} relaxivities about four times higher than the values observed in the same conditions for the commercial Contrast Agents (CAs) ProHance or Omniscan, regardless of the stabilizing agent used, while nanoparticles of Prussian blue and its analogues $M^{2+}/[Fe(CN)_6]^{3-}$ (M = Ni, Cu, Fe) present relatively modest values. The influence of the chemical composition of the nanoparticles, their crystal structure, spin values of lanthanide and transition metal ions, and stabilizing agent on the relaxivity values are investigated and discussed.

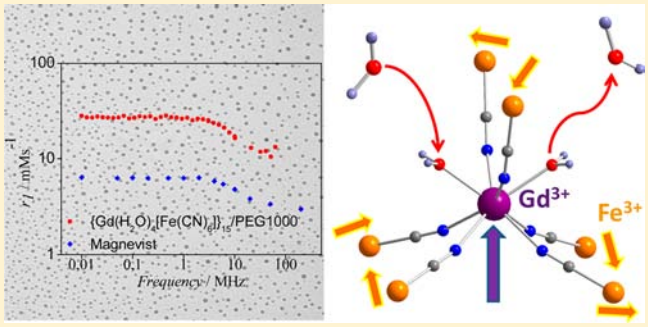

1. INTRODUCTION

Coordination polymer nanoparticles are a new type of inorganic nanomaterials, which are the subject of increasing interest due to their specific molecule-based nature that is different compared to other inorganic nano-objects.[1] They offer all the advantages of bulk molecular-based materials, such as determined and flexible molecular structures, adjustable physical and chemical properties, porosity, low density, and the ability to combine multiple properties in the same multifunctional nano-object. Furthermore, as their bulk molecule-based analogues, the coordination polymer nanoparticles can be obtained from molecular precursors through self-assembly reactions at room temperature. On the other hand, the use of appropriate stabilizing agents or matrixes allows the design of such nanoparticles with control over their size and shape at the nanometer scale and thus enables us to control and adjust their physical and chemical properties. The most investigated nanosized coordination polymers belong to the Metal−Organic Frameworks (MOFs)[1c,2] and to cyano-bridged coordination polymers also known as Prussian blue and its analogues.[3] Both families are based on lanthanides and/or transition metal ions connected by bridging carboxylates, phosphates, cyanides, or others ligands and provide useful magnetic, optical, and/or host−guest properties that are promising for various applications. In particular, some of these nano-objects in aqueous solutions stabilized by biocompatible ligands or polymers are the subject of increasing interest for applications in the biomedical field as nanocarriers for drug

Received: July 8, 2013
Published: November 18, 2013

   dx.doi.org/10.1021/ic401710j | Inorg. Chem. 2013, 52, 13402−13414

Scheme 1. Schematic Representation of the Self-Assembly Reaction for the Synthesis of Nanoparticles 1−7 with General Formula $Gd(H_2O)_4[Fe(CN)_6]$ or $M_3[Fe(CN)_6]_2{\cdot}xH_2O$ with the Three Kinds of Stabilizing Agents Used:[a]

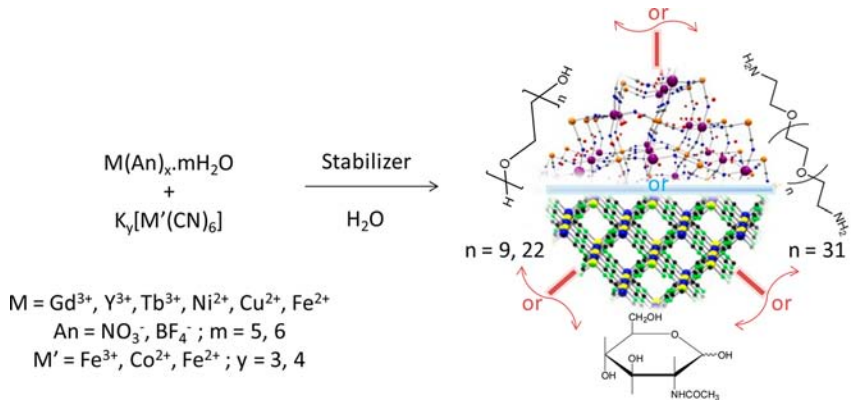

[a]Polyethylene glycols (n = 9 for PEG400 and n = 22 for PEG1000), polyethylene glycol modified with amine functional groups in terminal position (n = 31, PEG-NH_2) and N-acetyl-D-glucosamine (NADG).

delivery,[4] Contrast Agents (CAs) for X-ray Computed Tomography,[5] optical biomarkers,[2a,6] or therapeutic agents.[7] Among these, particular attention has been focused on the design of CAs made from new nanosized coordination polymers for Magnetic Resonance Imaging (MRI) because they can potentially compete with commercial products currently used in clinical practices.

MRI is a powerful noninvasive imaging technique of modern medicine used to visualize internal body structures.[8] The basic physical principle of Nuclear Magnetic Resonance (NMR) imaging consists of the application of magnetic field gradients to encode the signal in all three spatial directions. The NMR signal can be weighted by the water density and the longitudinal (T_1) and/or transverse (T_2) relaxation times of the tissues.[9] CAs are currently used in order to improve image contrast by locally increasing the nuclear relaxation rates.[10] Their efficiency is usually evaluated on the basis of their ability to influence the longitudinal, r_{1p}, and transverse, r_{2p}, proton relaxivities, and the r_{2p}/r_{1p} ratio that determine the action of the CA on the Magnetic Resonance (MR) image. For $r_{2p}/r_{1p} < 2$, the CA is positive, called T_1-relaxing, and provides a brilliant spot where it is delivered. Mononuclear complexes of paramagnetic Gd^{3+} are the commercial positive CAs most widely used, accounting for 60% of routine clinical MRI analyses. For example, currently used commercial positive CAs based on gadolinium chelate complexes called ProHance (or Gadoteridol) or Omniscan (or Gadodiamide) have r_1 values of about 3−5 $mM^{-1}\ s^{-1}$ at 20 MHz and 298 K.[11] For $r_{2p}/r_{1p} > 2$, the CA is negative, called T_2-relaxing, and provides a dark signal where it is localized in the tissues. Such a case is usually obtained when using superparamagnetic iron-based nanoparticles. In recent years, extensive fundamental and industrial research focused on the development of new efficient CAs with an increased effect on the protons' relaxivity allowing administration at a lower dose or imaging of low-concentration targets. In this respect, new families of T_1 CAs with improved relaxivity and local contrast effects were developed by the covalent anchoring of Gd^{3+} complexes to various nanostructures, polymers, dendrimers, or liposomes,[12] or by design of Gd^{3+}-based nanoparticles.[13]

Concerning nanosized coordination polymers, numerous MOFs-based nanoobjects, such as porous gadolinium-,[2,14] iron-,[15] manganese(II)-,[16] and lanthanide-based[17] nanoparticles of relatively large size (>50 nm) were identified as promising CAs for MRI to the extent that they present high r_1 or r_2 relaxivity values. Surprisingly, the family of cyano-bridged coordination polymers at the nanoscale has received less attention in this respect despite significant advances in the synthesis in aqueous solution of nano-objects of controlled size ranging from few to several hundred nanometers, including the use of water-soluble polymers, biopolymers, or biocompatible ligands.[18] There may be mentioned few investigations carried out on nanoparticles of Prussian blue,[19−21] Prussian blue doped with gadolinium ions,[23] or recently patented Mn(II)-containing Prussian blue analogues[22] with the aim to develop new T_1- or T_2-relaxing CAs for MRI. In this respect, Prussian blue nanoparticles of about 13 nm, stabilized by citric acid and conjugated with the 5-(aminoacetamido) fluorescein dye, exhibit modest relaxivity values of r_1 = 0.079 $mM^{-1}\ s^{-1}$ and r_2 = 0.488 $mM^{-1}\ s^{-1}$ at 1.5 T (with r_2/r_1 = 6.1) compared to commercial Gd^{3+}-based CAs.[19,20] However, these nanoparticles have a much higher stability in a wide pH range (from 2 to 7.5) and a much lower toxicity in contrast to mononuclear Gd^{3+} complexes. Furthermore, the Gd^{3+}-doped Prussian blue nanoparticles provide improved r_1 values higher by 1 to 2 orders of magnitude than the that of the commercial CAs.[23] Recently, some of us have investigated $Gd^{3+}/[Fe(CN)_6]^{3-}$ nanoparticles coated with chitosan exhibiting longitudinal relaxivity values six times higher than those of the clinically approved paramagnetic Gd^{3+} chelate complexes over the whole frequency range studied.[24,25] These results demonstrate the significant potential of these cyano-bridged coordination polymers as CAs for MRI. However, the animal origin of the chitosan matrix as well as the acidic pH of these solutions are significant disadvantages for application in the biomedical field.

In this manuscript, we present the synthesis, characterization, and ^1H NMR relaxometry properties for a series of ultrasmall cyano-bridged coordination polymer nanoparticles $Ln^{3+}/[M(CN)_6]^{3-}$ (Ln = Gd, Tb, Yb; M = Fe and Co) stabilized in aqueous solutions by biocompatible stabilizing agents. These 2−3.4 nm nanoparticules are stabilized by polyethylene glycols of different molecular weights, polyethylene glycol functionalized with amine groups, or by N-acetyl-D-glucosamine. Specific attention is devoted to the study of the influence of various parameters on the relaxivity that are the chemical composition of nanoparticles, their crystal structure, the electronic spin values of lanthanide and transition metal ions, as well as the nature of the stabilizing ligand.

dx.doi.org/10.1021/ic401710j | Inorg. Chem. 2013, 52, 13402−13414

Table 1. Some Relevant Characteristics of the Samples 1−4

sample	composition	M^{n+}/M'^{m+} ratio[a]	IR, ν(CN), cm^{-1}	nanoparticle size,[b] nm
1a	$Gd^{3+}/[Fe(CN)_6]^{3-}$@PEG400	0.97	2150, 2139, 2117, 2096, 2065	2.1 ± 0.9
1b	$Gd^{3+}/[Fe(CN)_6]^{3-}$@PEG1000	1.04	2150, 2140, 2070	2.5 ± 0.8
1c	$Gd^{3+}/[Fe(CN)_6]^{3-}$@$PEGNH_2$	1.02	2150, 2140, 2108, 2066	2.3 ± 0.7
1d	$Gd^{3+}/[Fe(CN)_6]^{3-}$@NADG	1.03	2150, 2139, 2108, 2098, 2065	3.4 ± 0.7
2	$Gd^{3+}/[Co(CN)_6]^{3-}$@PEG400	1.08	2152, 2139, 2107, 2096, 2069	2.4 ± 0.8
3	$Tb^{3+}/[Fe(CN)_6]^{3-}$@PEG400	1.05	2151, 2140, 2109, 2098, 2066	2.8 ± 1.0
4	$Y^{3+}/[Fe(CN)_6]^{3-}$@PEG400	0.87	2151, 2111, 2099, 2066	3.0 ± 0.8

[a]Calculated from elemental and EDS analyses. [b]Determined from TEM measurements.

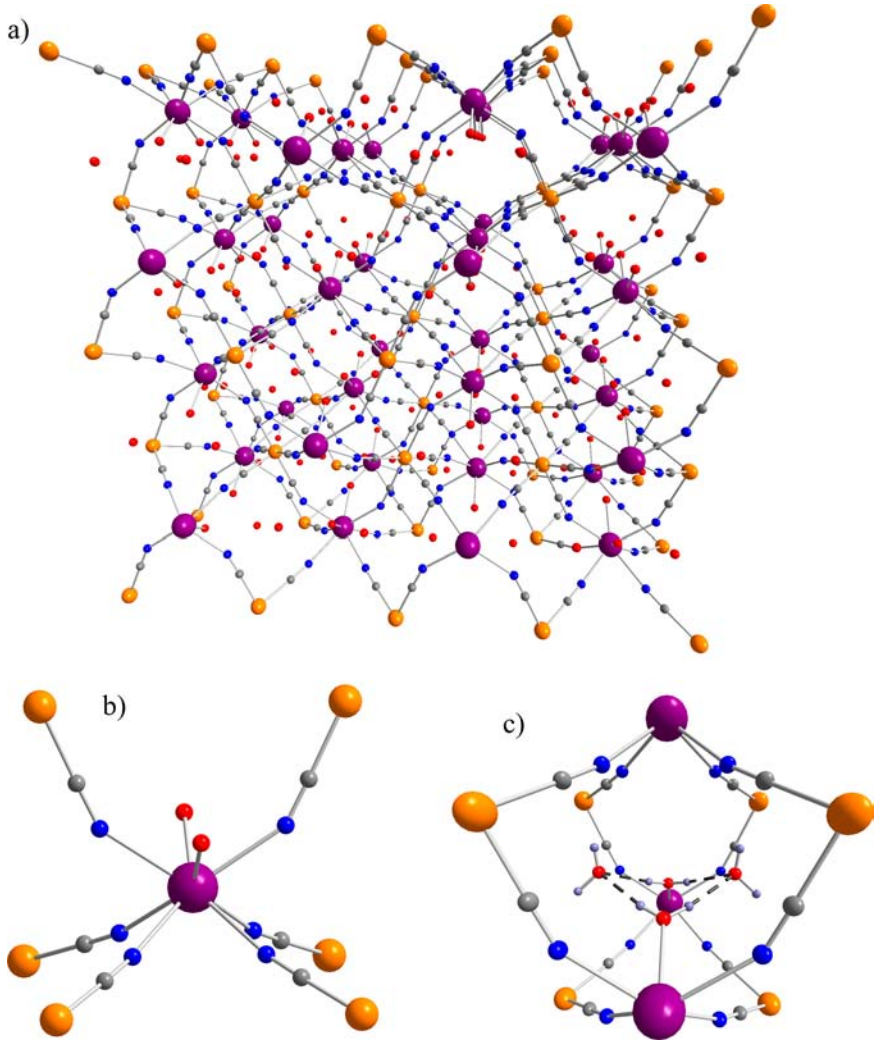

Figure 1. (a) Perspective views of the neutral three-dimensional $_\infty{}^3[Gd(H_2O)_4Fe(CN)_6]$ network showing the coordinated and crystallized water molecules (Gd ion is represented in violet, Fe is in orange, N is in blue, O is in red, and C is in gray). (b) Representation of the average square anti-prism $\{GdN_6O_2\}$ coordination environment of the Gd^{3+} center composing the crystal structure of $Gd(H_2O)_4[Fe(CN)_6]$. (c) Perspective view of a pore containing the cluster of hydrogen bonded water molecules (dashed lines).

2. RESULT AND DISCUSSION

2.1. Synthesis, Structural, and Textural Characterizations. Nanoparticles of cyano-bridged coordination polymers are obtained by self-assembly reaction in water between an hexacyanometallate precursor $[M(CN)_6]^{3-}$ (M = Fe, Co) and a lanthanide (Gd^{3+}, Tb^{3+} or Y^{3+}) or divalent (Ni^{2+}, Cu^{2+}, Fe^{2+}) transition metal ion in the presence of a stabilizing agent such as nonfunctionalized polyethylene glycol (PEG) of different molecular weights (PEG400 and PEG1000), polyethylene glycol having terminal amino groups (PEG-NH_2), or a glucose derivative, N-acetyl-D-glucosamine (NADG) (Scheme 1). These stabilizing agents have been chosen because they (i) are soluble in water at physiological pH; (ii) are biocompatible; (iii) should permit stabilizing the nanoparticles in aqueous solutions and avoid the nanoparticles aggregation; (iv) should increase the blood circulation time of the nanoparticles and prevent macrophage action if the nanoparticles are used as contrast agent. PEG400 and PEG1000 have no functional groups permitting their covalent anchoring to the nanoparticles' surface, while $PEGNH_2$ and N-acetyl-D-glucosamine presents terminal

dx.doi.org/10.1021/ic401710j | Inorg. Chem. 2013, 52, 13402−13414

coordination groups potentially able to anchor covalently the stabilizers to the nanoparticles' surface. In addition, the latter as a glucose derivative may potentially be interesting as targeting ligand. The presence of a stabilizing agent during the synthesis prevents infinite growth of the tridimensional cyano-bridged coordination polymer network by coordination of the surface metallic ions and/or entrapment leading to the formation of stable colloidal solutions. The series of nanoparticles of different chemical compositions **1**−**7** (Table 1) obtained by this synthetic route with the various stabilizers covered by this study are shown in Table 1. The self-assembly reaction synthesis of Gd^{3+}/$[Fe(CN)_6]^{3-}$@Stabilizer nanoparticles with PEG400 **1a**, PEG1000 **1b**, PEG-NH_2 **1c**, and NADG **1d** leads in all cases to yellow solutions from which the nanoparticles were precipitated by addition of a nonsolvent such as methanol or acetone, then washed and redispersed in water in the presence of few drops of the corresponding stabilizer. Note that these colloidal solutions remain stable in the dark for several weeks without flocculation. Elemental and EDS analyses show that the Gd^{3+}/Fe^{3+} ratio is close to *ca.* 1 (Table 1), the expected value for the bulk compound of formula $Gd(H_2O)_4[Fe(CN)_6]$.[26] To study the influence of the nature and electronic spin of lanthanide and transition metal ions on the size and shape of the nanoparticles, and the resulting relaxivity properties, we also used the diamagnetic cyanometallate precursor $[Co(CN)_6]^{3-}$ instead of $[Fe(CN)_6]^{3-}$ and other lanthanides, Tb^{3+} or Y^{3+}, than Gd^{3+}. When the $[Fe(CN)_6]^{3-}$ precursor having the Fe^{3+} ion with $S = 1/2$ is replaced by the diamagnetic $[Co(CN)_6]^{3-}$ one, sample $Gd^{3+}/[Co(CN)_6]^{3-}$@PEG400 **2** is obtained. The Tb^{3+} ion having an effective $S = 1/2$ with high magnetic anisotropy ($g_\perp = 10$, $g_\parallel = 0$) and the diamagnetic Y^{3+} ion used instead of Gd^{3+} gave samples $Tb^{3+}/[Fe(CN)_6]^{3-}$@PEG400 **3** and $Y^{3+}/[Fe(CN)_6]^{3-}$@PEG400 **4**, respectively. As in the previous cases, the Ln^{3+}/M'^{3+} ratio for these samples is almost equal to 1 (Table 1). The synthesis of nanoparticles of $M^{2+}/[Fe(CN)_6]^{3-}$@Stabilizer (with $M^{2+} = Ni^{2+}$ for **5** or $M^{2+} = Cu^{2+}$ for **6** with Stabilizer = PEG1000) and $Fe^{2+}/[Fe(CN)_6]^{3-}$@PEGNH_2 **7** were also performed in the same way, but using different stoichiometric amounts (see Experimental Section). The M^{2+}/Fe^{3+} ratio equals 1.48 for Ni-containing nanoparticles **5** and 1.45 for Cu-containing nanoparticles **6**, which is close to the expected value of 1.5 observed for the corresponding bulk materials of formula $M_3[Fe(CN)_6]_2{\cdot}xH_2O$ (Table S1).

For all samples, FTIR spectroscopy confirms the formation of a cyano-bridged network as is attested by the higher wavenumber values in the cyanide stretching region with respect to the hexacyanometallate precursors. For $Ln^{3+}/[M'(CN)_6]^{3-}$@Stabilizer (Ln = Gd, Tb, Y; M′ = Fe, Co) nanoparticles **1**−**4**, the cyanide region consists of five bands located around 2066, 2108, 2117, 2140, and 2150 cm^{-1} (Table 1). These values are similar to values previously reported for the bulk coordination network $Tb(H_2O)_4[Fe(CN)_6]$ (i.e., 2066, 2108, 2121, 2140, and 2151 cm^{-1}).[26] The lowest values can be ascribed to the terminal cyanides M^{III}-CN, while those highest come from the bridging cyanides Fe^{III}-CN-Ln^{III}. Concerning the $Ni^{2+}/[Fe(CN)_6]^{3-}$@Stabilizer **5** and $Cu^{2+}/[Fe(CN)_6]^{3-}$@Stabilizer **6** Prussian blue analogues nanoparticles, two bands are located in the region of cyanides at ca. 2119 and 2170 cm^{-1} (Table S1). While the latter can be ascribed to the Fe^{3+}-CN-M^{2+} stretching vibration, the former may originate from the linkage isomerization with a Fe^{3+}-NC-M^{2+} coordination mode, as it was reported for the bulk cyano-bridged coordination polymer.[27] The Prussian blue nanoparticles **7** exhibit a single characteristic band located at 2075 cm^{-1}, as observed for the bulk material.[28] For all samples, the presence of the stabilizing agent is confirmed by the observation of C−H stretching vibrations bands in the 2800−2950 cm^{-1} region.

The powder X-ray diffraction (PXRD) patterns of all nanoparticles' samples were collected at room temperature further confirming the formation of cyano-bridged coordination networks. The PXRD patterns obtained for the nanoparticles of lanthanide hexacyanometallates **1**−**4** are comparable with the diffraction pattern obtained for the bulk compound $Gd(H_2O)_4[Fe(CN)_6]$.[26] The crystal structure of the tridimensional coordination network $Gd(H_2O)_4[Fe(CN)_6]$ is shown in Figure 1a (see SI for the details of the single crystal structure, Table S2). The compound crystallizes in the orthorhombic system with *Cmcm* space group and cell parameters equal to $a = 7.4016(3)$ Å, $b = 12.7813(14)$ Å, and $c = 13.5980(12)$ Å. The asymmetric unit is composed of two crystallographically independent metal ions, Gd^{3+} and Fe^{3+}. The coordination sphere of the Gd^{3+} centers consists of six nitrogen belonging to cyanide groups plus two coordinated water molecules leading to an environment $\{GdN_6O_2\}$ describing a slightly distorted square anti-prism with Ln−(N,O) bond lengths ranging from 2.363(1) to 2.495(2) Å (Figure 1b). This coordination geometry is typical for Gd^{3+} ion.[29] The coordination sphere of the Fe^{3+} ions consists of six carbon atoms from six cyanide ligands leading to an octahedral geometry. Intermetallic connectivity is provided via the μ_2-cyanide bridges, leading ultimately to the formation of a neutral three-dimensional $_\infty{}^3[Gd(H_2O)_2Fe(CN)_6]{\cdot}2H_2O$ network (Figure 1a). Connectivity between three gadolinium(III) and six iron(III) metal ions creates distorted pores having an approximate dimension of 7.40 Å × 5.35 Å × 7.38 Å and containing two crystallized water molecules. Directional and strong hydrogen bonds ($d_{O\cdots O}$ = 2.802(2); angle O−H···O = 169.43°) are present between the crystallized and coordinated water molecules forming a cluster of four water molecules within the pore (Figure 1c). The PXRD pattern of the sample **1a** is presented in Figure 2 as an example. Varying the lanthanide ion (by Tb^{3+} **3** or Y^{3+} **4**) as well as the cyanometallate complex ($[Co(CN)_6]^{3-}$ **2**) does not modify significantly the diffractogram pattern and therefore confirms that these compounds are isostructural (Figure S1, SI).

The PXRD patterns of nanoparticles $Ni^{2+}/[Fe(CN)_6]^{3-}$@Stabilizer **5** are comparable to those obtained for the

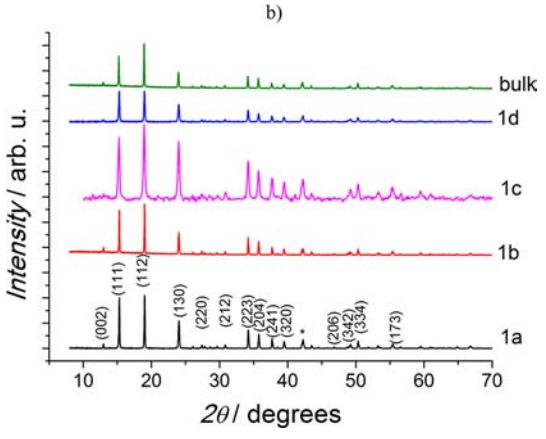

Figure 2. Room temperature PXRD patterns for samples **1a**−**1d** indexed using the space group *Cmcm* as well as for the bulk analogous $Gd(H_2O)_4[Fe(CN)_6]$.

dx.doi.org/10.1021/ic401710j | *Inorg. Chem.* 2013, 52, 13402−13414

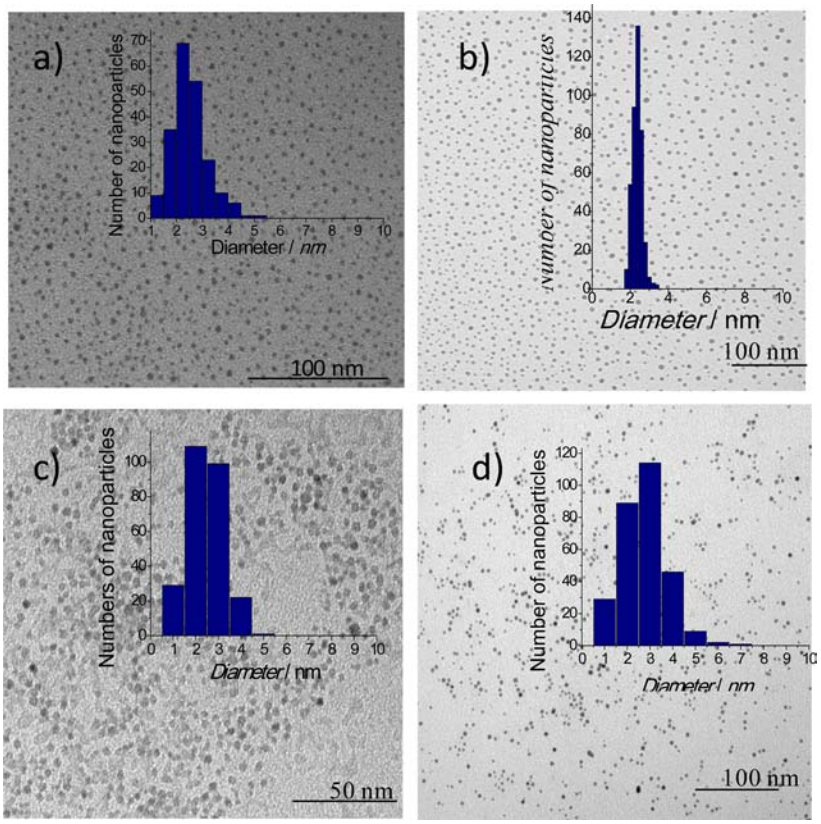

Figure 3. TEM images of nanoparticles and the corresponding histograms of the nanoparticle's size distribution (inset) for (a) $Gd^{3+}/[Fe(CN)_6]^{3-}$@PEG400 **1a**; (b) $Gd^{3+}/[Fe(CN)_6]^{3-}$@PEG1000 **1b**; (c) $Gd^{3+}/[Co(CN)_6]^{3-}$@PEG400 **2**; and (d) $Tb^{3+}/[Fe(CN)_6]^{3-}$@PEG400 **3**.

Table 2. Relaxivity and Magnetic Properties for Samples 1−7[a]

sample	composition	r_1, $s^{-1}.mM^{-1}$	r_2, $s^{-1}.mM^{-1}$	r_2/r_1	χT_{calc}.emu.K.mol^{-1}[b]	χT_{exp}, emu.K.mol^{-1}[c]
	ProHance (Gadoteridol)	3.5 ± 0.1	5.4 ± 0.1	1.53	7.875	-
1a	$Gd^{3+}/[Fe(CN)_6]^{3-}$@PEG400	12.6 ± 0.1	15.0 ± 0.1	1.20	8.25	7.73
1b	$Gd^{3+}/[Fe(CN)_6]^{3-}$@PEG1000	13.3[b]	20.1[b]	1.50	8.25	7.80
1c	$Gd^{3+}/[Fe(CN)_6]^{3-}$@$PEGNH_2$	11.2 ± 0.1	12.2 ± 0.2	1.09	8.25	7.92
1d	$Gd^{3+}/[Fe(CN)_6]^{3-}$@NADG	9.9 ± 0.1	13.1 ± 0.4	1.33	8.25	7.95
2	$Gd^{3+}/[Co(CN)_6]^{3-}$@PEG400	4.8 ± 0.1	5.5 ± 0.1	1.14	7.87	7.41
3	$Tb^{3+}/[Fe(CN)_6]^{3-}$@PEG400	0.11 ± 0.03	2.7 ± 0.3	24.18	11.2	10.95
4	$Y^{3+}/[Fe(CN)_6]^{3-}$@PEG400	0.01 ± 0.01	0.05 ± 0.03	5.00	0.375	0.43

[a]Relaxivity values obtained at 300 K under a 4.7 T applied magnetic field. [b]Calculated based on the bulk compounds $Ln(H_2O)_4[Fe(CN)_6]$. [c]Measured at 300 K at 60 mHz.

corresponding bulk compounds (*fcc* structure of the bulk $Ni_3[Fe(CN)_6]_2{\cdot}15H_2O$, JCPDS 01−082−2283, Figure S2, SI) with a constant lattice parameter a = 10.16 Å close to that of bulk materials of 10.22 Å (Figure S3, SI).[30] The bulk Prussian blue analogues have three-dimensional coordination networks in which the hexacyanoferrate moieties are connected to divalent metals in a face-centered cubic structure. The packing arrangement reveals the presence of vacant sites in the crystal lattice due to missing $[Fe(CN)_6]^{3-}$ units in order to ensure the electroneutrality. These interstitial sites are occupied by crystallized water molecules. Some bivalent metal sites (such as Ni(II)) situated in the vicinity of the vacant sites are coordinated to less than six cyanide groups and their coordination sphere is complemented with water molecules to maintain the octahedral geometry. The presence of hydrogen bonds between coordinated and crystallized water molecules results in a three-dimensional network of hydrogen bonds leading for instance to the observation of high proton conductivity.[31] A similar crystal structure is found for nanosized Prussian blue analogue $Cu^{2+}/[Fe(CN)_6]^{3-}$@PEG1000 **6** and Prussian blue $Fe^{3+}/[Fe(CN)_6]^{4-}$@$PEGNH_2$ **7** with a lattice parameter constant a = 10.30 Å and a = 10.15 Å, respectively (Figure S3, SI).

Transmission Electronic Microscopy (TEM) measurements were used to investigate the size and morphology of the nanoparticles obtained. Representative TEM micrographs of $Ln^{3+}/[M(CN)_6]^{3-}$@Stabilizer nanoparticles **1**−**4** are given in Figure S4 as examples.

Whatever the composition of the lanthanide hexacyanometallate network and the nature of the stabilizing agents, the nanoparticles are spherical in shape with no sign of aggregation. The mean size of the nanoparticles ranges from 2.1 to 3.4 nm (Table 1) indicating that the nature of the lanthanide or cyanometallate complex and the nature of the stabilizing agent have little influence thereon.

In a similar way, $Ni^{2+}/[Fe(CN)_6]^{3-}$@PEG1000 **5** and $Cu^{2+}/[Fe(CN)_6]^{3-}$@PEG1000 **6** nanoparticles present a spherical

dx.doi.org/10.1021/ic401710j | *Inorg. Chem.* 2013, 52, 13402−13414

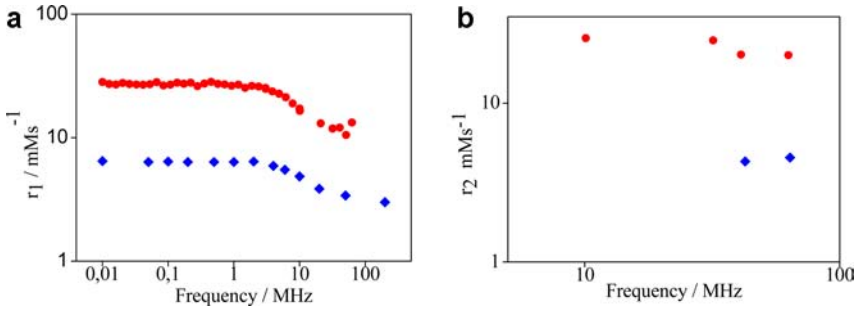

Figure 4. (a) Longitudinal and (b) transverse relaxivities of sample **1b** (red) collected at $T \approx 25$ °C and compared to the same quantity reported for the commercial compounds Magnevist (blue) for (a) and Omniscan (blue) for (b).

shape with mean size values ranging from 3.0 to 5.5 nm (Table S1, Figure S5). The nanoparticles of Prussian blue **7** are smaller with mean size equal to 1.4 ± 0.4 nm. In all cases, the nanoparticles are nonaggregated and well dispersed in water.

The magnetic characterizations of as-obtained nanoparticles were performed on powders of nanoparticles using a SQUID-MPMS-XL magnetometer operating in the temperature range 1.8−350 K and up to 7 T using dc (direct current) and ac (alternating current) modes. The temperature dependence of magnetization and $1/\chi$ performed for the sample **1b** with an applied field of 0.1 T are shown Figure S6 as an example. At 300 K, the χT value of 7.80 emu K mol^{-1} is close to that calculated one of 8.25 emu K mol^{-1} for noninteracting Gd^{3+} ($S = 7/2$ with ground state $^8S_{7/2}$, 7.875 emu K mol^{-1}) and Fe^{3+} ($S = 1/2$, 0.375 emu K mol^{-1}) ions (Table 2). As the temperature decreases, $1/\chi$ decreases linearly to zero indicating a pure paramagnetic behavior. However, the χ' and χ'' components of the ac magnetic susceptibility show an abrupt increase below 1.8 K indicating the beginning of a magnetic transition below this temperature. Due to the absence of a clear maximum on these curves, it is difficult to determine the nature of this anomaly and the possible associated transition (Inset of Figure S6). The nanoparticles **1a−d** present similar paramagnetic behavior due to their similar size and composition. Samples **2−4** obtained by replacing the Gd^{3+} by other lanthanides or Fe^{3+} with Co^{3+} also behave as paramagnets. χT values measured at 300 K with an applied magnetic field of 4.7 T are given in Table 2. In all cases, these values are slightly lower than those calculated which may be explained by the fact that the molecular weight of nanoparticles is underestimated due to the presence of the stabilizing agents.

The nanoparticles $Ni^{2+}/[Fe(CN)_6]^{3-}$@PEG1000 (**5**) and $Cu^{2+}/[Fe(CN)_6]^{3-}$@PEG1000 (**6**) and $Fe^{3+}/[Fe(CN)_6]^{4-}$@$PEGNH_2$ (**7**) have superparamagnetic behavior modified by the presence of interparticle dipolar interactions leading to a spin-glass transition at low temperature (Table S3, Figures S7 and S8, SI). However, they are paramagnetic at 300 K and the measured room temperature χT values at 4.7 T are given in Table S4. As in the previous cases, the obtained values are slightly lower than those calculated due to the presence of the stabilizing agents.

2. 2. Relaxivity measurements. The relaxivity (i.e., the change of nuclear relaxation rate per unit concentration of magnetic center) of a CA is an important measure to evaluate its efficiency in improving the contrast of a MR image. The longitudinal, T_1, and transverse, T_2, proton relaxation times, from which relaxivities are calculated (see below), can be written as the sum of three contributions from the physical mechanisms of the inner sphere, the outer sphere, and the second coordination sphere, which induce accelerated relaxation. Such relaxation times depend on numerous parameters such as (i) the value of the effective electron spin of the paramagnetic center and its reversal frequency $1/\tau_{ei}$ ($i = 1, 2$), where τ_{e1} and τ_{e2} are the electronic correlation times; (ii) the number of the paramagnetic sites in the complex or the nanoparticle; (iii) the chemical environment of the metal ion; (iv) the number q (hydration number) of coordinated water molecules; (v) the chemical exchange rate $1/\tau_{ex}$ (τ_{ex} is the exchange correlation time) between the water molecules coordinated to the paramagnetic center and bulk water; (vi) the diffusion rate of water molecules $1/\tau_d$ (τ_d is the diffusion time); (vii) the size of the CA which influences the rotational correlation time τ_R of the "water-paramagnetic ion" complex formed, and so on.

For T_1-relaxating CAs, only the theory concerning the so-called aqua-ion paramagnetic systems (derived from the Bloembergen-Purcell-Pound (BPP) or Solomon-Bloembergen-Morgan (SBM) theory)[32] including small mononuclear Gd^{3+} complexes allows to interpret correctly the experimentally observed r_1 behavior. For more complex systems such as nanoparticles, the interpretation of experimental data within a theoretical framework is quite difficult. For this reason, in this work, we focus on the relaxometry measurements (and related nuclear relaxation times) of a series of cyano-bridged coordination polymer nanoparticles of different chemical composition with paramagnetic centers of different spin value and anisotropy, as well as different stabilizing agents, to attempt a qualitative explanation of the results observed and correlate them with the magnetic properties.

Measurements of ^{1}H NMR longitudinal, T_1, and transverse, T_2, relaxation times at different frequencies ν (also leading to the plot of the NMR-Dispersion profile) at room temperature were performed on diluted solutions of samples **1a** (at $\nu = 200$ and 300 MHz) and **1b** (in the range 10 kHz $\leq \nu \leq$ 212 MHz for T_1 and 15 MHz $\leq \nu \leq$ 60 MHz for T_2). Note that the difference in T_1 and T_2 with respect to the values obtained at physiological temperature is within 10%. Using the measured T_1 and T_2 values, the efficiency of samples as MRI CAs was determined by calculating the nuclear relaxivities $r_{1,2}$, ($i = 1$ refers to longitudinal relaxivity, $i = 2$ to transverse relaxivity) as given by the following equation:[10,11]

$$r_{ip} = [(1/T_i)_{meas} - (1/T_i)_{dia}]/c \qquad i = 1, 2$$

where $(1/T_i)_{meas}$ is the measured value for the sample with a concentration c (mmol L^{-1}) of magnetic center (for instance 4 mmol L^{-1} of Gd^{3+} for **1b**), and $(1/T_i)_{dia}$ refers to the nuclear relaxation rate of the diamagnetic water. The longitudinal and transverse relaxivities measure the increase of, respectively, the nuclear spin−lattice and spin−spin relaxation rates (generally ^{1}H NMR) due to the presence of a magnetic system in the solvent

dx.doi.org/10.1021/ic401710j | Inorg. Chem. 2013, 52, 13402−13414

(water in general case), referring to a concentration of 1 mM of magnetic center.[10,11] The generation and detection of NMR signal was obtained with a Smartracer Stelar relaxometer (which uses the Fast-Field-Cycling technique) for 10 kHz $\leq \nu \leq$ 10 MHz,[33] a Stelar Spinmaster, and an Apollo-Tecmag FT-NMR spectrometers for $\nu >$ 10 MHz. In the second case, the standard radio frequency excitation sequences CPMG-like (T_2) and saturation-recovery (T_1) were used. In Figure 4 are reported the r_1 and r_2 measured values for sample **1b**, together with the respective values for Magnevist (Gd-DTPA) and Omniscan (Gadodiamide), depending on the measuring frequency. The longitudinal, r_1, relaxivity is frequency dependent, while the transverse relaxivity, r_2, does not show a strong frequency dependence. Such behavior is typical of small paramagnetic CAs.[34] Noticeably, the r_1 and r_2 relaxivities of sample **1b** are approximately four times higher than those of Omniscan/Magnevist over the whole frequency range.

For the nanoparticles $Gd^{3+}/[Fe(CN)_6]^{3-}$@PEG400 **1a**, proton T_1 and T_2 relaxation time measurements were performed on an aqueous solutions with different concentrations of nanoparticles at room temperature (300 K) and an applied magnetic field of 4.7 T using a Tecmag Apollo spectrometer operating at 200 MHz and at 7 T using a Bruker Pharmascan small animal MRI system operating at 300 MHz (see Experimental section). The rates observed for both longitudinal and transverse relaxations showed a linear dependence according to the nanoparticles' concentration. Using the inversion–recovery and spin echo (Carr-Purcell Meiboom Gill) sequences to measure T_1 and T_2, we calculated the longitudinal and transverse relaxivities from the slope of the plot of $1/T_1$ and $1/T_2$ curves vs nanoparticles' concentration. The results were, respectively, 12.6 ± 0.1 and 16.0 ± 0.1 mM^{-1} s^{-1} with the r_2/r_1 ratio equal to 1.26 (Table 2, Figure 5). The r_1 and r_2 values

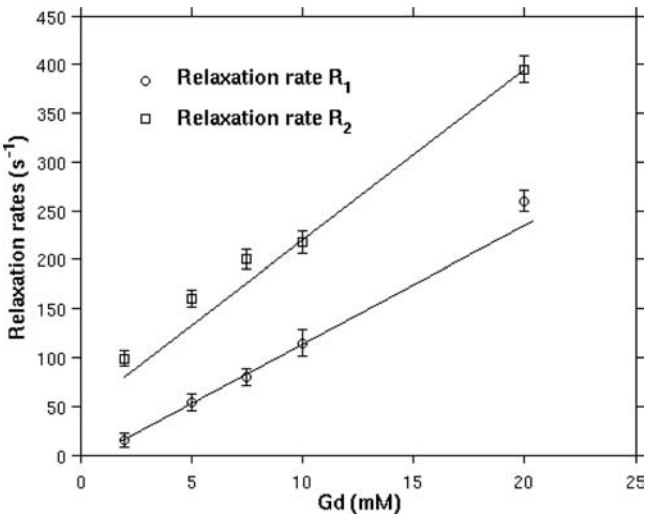

Figure 5. T_1 and T_2 relaxation rate measurements vs concentration of aqueous solutions of the nanoparticles **1a** performed at an applied magnetic field of 4.7 T.

measured at 7 T are close to the 4.7 T ones and equal to 12.1 ± 0.1 and 10.7 ± 0.1 mM^{-1} s^{-1}, respectively, with the r_2/r_1 ratio equal to 0.88 (Figure S10). The T_1 and T_2 relaxation time measurements of aqueous solutions of the commercial CA ProHance (Gadoteridol) carried out under the same conditions also showed a linear dependence as a function of the CA concentration and permitted us to determine its r_1 and r_2 relaxivities, in this case, equal to 3.5 ± 0.1 and 5.4 ± 0.1 mM^{-1} s^{-1} at 4.7 T and 3.00 ± 0.01 and 3.41 ± 0.01 mM^{-1} s^{-1} at 7 T (Figure S11). The obtained results indicate that the nanoparticles' sample **1a** is essentially a T_1-relaxing agent and causes an increase in the NMR signal four times higher than the Gadoteridol commercial agent. Note also that the r_1 values measured at 4.7 and 7 T are close.

The influence of the stabilizing agent on the relaxivity properties was studied by comparing samples **1a–d** which have the same inorganic core composition $Gd^{3+}/[Fe(CN)_6]^{3-}$ with nanoparticles of similar size coated with the different stabilizers used in this study. It appears that the measured values of r_1 and r_2 at 4.7 T are in the range 10–13 and 10.6–16.0 mM^{-1} s^{-1} (Table 2, Figure S12), respectively, indicating no influence on the nature of the stabilizer and their anchor mode at the surface of the nanoparticles. These results suggest that water exchange inducing T_1 relaxation occurring on accessible Gd^{3+} sites is little influenced by the ligands situated on the surface of the nanoparticles.

As a further check on the ability to improve the MRI contrast of these compounds, we collected MRI images of vials containing the sample solutions **1a**. T_1- and T_2-weighted MRI slices of aqueous solutions of nanoparticles **1a** with varying concentrations ranging from 0.5 to 10.6 mM were performed using a 7 T Bruker Pharmascan spectrometer (Figure 6). The T_1 images become progressively brighter as the concentration of nanoparticles **1a** increases; then, the signal decreases as the concentration becomes higher, thus allowing an order of magnitude of the most suitable concentrations for use in MRI (Figure 6a). On the other hand, as expected, the T_2-weighted images become darker when the concentration increases (Figure 6b). These results confirm for the first time the potential of $Gd^{3+}/[Fe(CN)_6]^{3-}$ nanoparticles as a T_1 CA in MRI.

Let us now consider the different sources of nuclear relaxation responsible for the increase in relaxation rates and, as a consequence, high nuclear relaxivities (especially r_1 for positive paramagnetic agents). It is well-known that the presence of Gd^{3+} ions makes the CA particularly efficient because the Gd^{3+} ion has a high electronic spin (S = 7/2) with a low longitudinal electronic-spin relaxation rate at the imaging magnetic field.[34] However, as we mentioned before, it is quite difficult to provide the theoretical explanations for the relaxivity properties of complex systems containing not only Gd^{3+} ions, but also other paramagnetic centers (such as Fe^{3+}) assembled in a nanoparticle. Various parameters related to the chemical environment of Gd^{3+} and the second paramagnetic ion, their spins, crystal structure of the nanosized network, the chemical exchange with water, water accessibility to paramagnetic centers, and the nanoparticles' size should be taken into account.

The first parameter to consider is the presence of coordinated water (r_1 and r_2 in the mechanism of the inner sphere are proportional to the number q of such molecules) at the Gd^{3+} paramagnetic centers of the nanoparticles and the possibility of water exchange. The water exchange rate $1/\tau_{ex}$ to be effective in accelerating the nuclear relaxation must be in the region of MHz. The previously described crystal structure of the $Gd(H_2O)_4[Fe(CN)_6]$ three-dimensional coordination network shown in Figure 1 offers all the required parameters: (i) the structure has covalently bonded paramagnetic Gd^{3+} (S = 7/2) and Fe^{3+} (S = 1/2) metal ions leading to nanoparticles with a paramagnetic behavior and a relatively high magnetic moment; (ii) each Gd^{3+} site of the structure has two coordinated water molecules (q = 2) in the inner coordination sphere that can potentially be

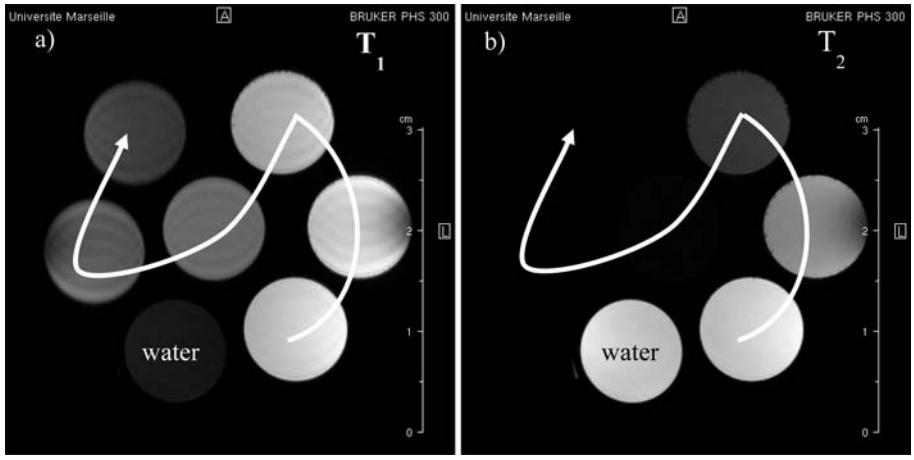

Figure 6. (a) T_1-weighted and (b) T_2-weighted MRI slices of aqueous solutions of **1a** with varying concentrations. The arrow indicates the direction of increasing concentration: 0, 0.5, 1, 2, 5, 7.5, and 10.6 mM.

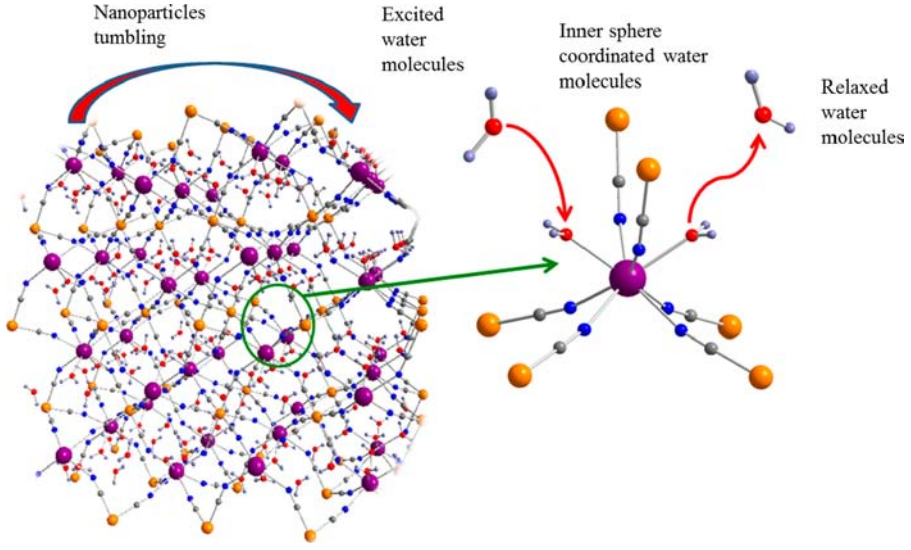

Figure 7. Schematic representation of a possible pathway for water exchange in the $Gd^{3+}/[Fe(CN)_6]^{3-}$ nanoparticles.

exchanged; (iii) two crystallized water molecules situated in the channels of the structure linked through hydrogen bonds to the coordinated water; (iv) the presence of large pores that can permit easy diffusion of small molecular species such as water; and (v) due to the formation of hydrogen-bonded water clusters in the pores, the diffusion and exchange of coordinated water molecules with bulk water should be effective. Figure 7 represents schematically a possible pathway of water exchange in $Gd(H_2O)_4[Fe(CN)_6]$ nanoparticles involving coordinated and crystallized water molecules.

The second group of parameters to be considered is the size of the nanoparticles which can govern the complex influence of the number of paramagnetic Gd^{3+} and Fe^{3+} ions within the CA, the surface-to-volume ratio, and the molecular rotation of the complex "water−paramagnetic site". It is commonly assumed that in the case of nanoparticles with an increasing number of paramagnetic centers compared to currently used commercial CAs containing only one Gd^{3+}, the higher local concentration of paramagnetic ions improves the local image contrast in the region of interest. For nanoparticles **1a−d** having sizes in the range 2−3 nm, the number of paramagnetic Gd^{3+} and Fe^{3+} ions estimated taking into account the size and cells parameters is about 40−50 per nanoparticle. For instance, the chemical composition of the nanoparticle **1a** of 2.10 nm is $\{Gd(H_2O)_4[Fe(CN)_6]\}_{15}$. For such small nanoparticle size, the paramagnetic centers should mainly be localized at the surface that offers their accessibility and facilitates the water exchange. The SBM theory of paramagnetic relaxivity also predicts that the relaxivity of a Gd^{3+} complex with optimal fast rate of water exchange (k_{exch} = 10^8 s^{-1}) can be increased drastically slowing its molecular tumbling. This can be achieved by increasing the molecular weight of the CA by conjugating the complex to a macromolecule or by assembling the Gd^{3+} ions into nanoparticles. The double enhancement in relaxivity over commercial CAs has previously been observed in the case of small Gd^{3+}-containing inorganic nanoparticles (<10 nm) and attributed mainly to the difference in their tumbling time: the molecular tumbling is in the range of nanoseconds for such small nanoparticles and of picoseconds for Gd^{3+} mononuclear complexes.[13e] In the same way, improved relaxivity (r_1 = 20−36 mM^{-1} s^{-1} at 3 T) was also observed with porous gadolinium-containing MOFs nanorods (around 100 nm in length and 40 nm in diameter). However, in both cases, the authors show the occurrence of an inverse dependence of r_1 value with the nanoparticles' size, which can be explained by reduction of surface areas for larger particles and decreased water accessibility to paramagnetic centers. Thus, the size of the

dx.doi.org/10.1021/ic401710j | Inorg. Chem. 2013, 52, 13402−13414

nanoparticles should be optimal to allow relatively slow molecular rotation (better to say, the rotational frequency $1/\tau_R$ must not be far from the Larmor frequency) on one hand and a good diffusion of water to the paramagnetic centers on the other. Consequently, slow molecular tumbling and a small nanoparticles size (2−3 nm) allowing water exchange at the Gd^{3+} ions located at surface and in the core of the $Gd^{3+}/[Fe(CN)_6]^{3-}$ nanoparticles may explain the increase in their r_1 relaxivity in comparison with commercial Gd^{3+} complexes.

To streamline our approach, we investigated the influence of other parameters on the nuclear relaxivity. For small Gd^{3+}-containing complexes, the relaxivity is directly proportional to the square of the effective magnetic moment of the paramagnetic center and hence is directly proportional to its χT value, but that is not obvious for nanoparticles. In order to clarify this, we tried to correlate the trend of relaxivity with magnetic susceptibility measurements performed at room temperature.

First of all, the influence of the magnetic nature (paramagnetic or diamagnetic) of the cyanometallate moiety was studied. For similar nanoparticle size, structure, stabilizing agent, and lanthanide ion (Gd^{3+}), changing the paramagnetic $[Fe(CN)_6]^{3-}$ complex ($3d^5$, $S = 1/2$) with the diamagnetic $[Co(CN)_6]^{3-}$ ($3d^6$, $S = 0$) one (sample **1a** and **2**, respectively) induces a decrease of the r_1 and r_2 values by 2.5× and 2×, respectively: the r_1 and r_2 values are equal to 4.8 and 5.5 mM^{-1} s^{-1} for **2** (Table 2, Figure S13a). This r_1 value decreases but remains higher than those of Gadoteridol and can be compared to the value of longitudinal relaxivity observed for ultrasmall $NaGdF_4$ nanoparticles of 2.5 nm.[13e] This suggests that the improvement of relaxivity compared to mononuclear complexes of Gd^{3+} is due to a cooperative effect of the increasing number of Gd^{3+} atoms, a possible surface effect and an accessibility of all Gd^{3+} sites (surface and core), and slowing of molecular tumbling. However, the r_1 value decreases by 2.5 times in comparison to that observed for nanoparticles **1**, clearly indicating not only that the electronic spin of the Gd^{3+} contributes to the high r_1 value, but also that the presence of another paramagnetic center connected via cyano-bridge to gadolinium strongly influences the proton relaxation. Note that only a slight decrease of the room temperature χT value from 7.73 (for **1a**) to 7.41 $cm^3.K.mol^{-1}$ (for **2**) (Table 2) is observed, suggesting that some other effect than just the presence of the electronic spin of a second paramagnetic ion is involved in the mechanism of relaxation, despite the weak exchange interaction expected for 3d-4f systems (less than 10 cm^{-1}).

Second, the influence of the Gd^{3+} ion was demonstrated by replacing it with another lanthanide ion keeping the structure of the cyano-bridged network of nanoparticles. In the case of the diamagnetic Y^{3+} ion (sample **4**), an almost complete vanishing for both relaxivities values was observed ($r_1 = 0.01$ and $r_2 = 0.05$ mM^{-1} s^{-1}, Table 2, Figure S13b). This may be correlated with a strong decrease of the χT value (0.43 $cm^3.K.mol^{-1}$) measured for nanoparticles **4** compared to the value obtained for nanoparticles **1**. To confirm this hypothesis, the strongly anisotropic Tb^{3+} ion ($S_{eff} = 1/2$, $g_\perp = 10$) with a higher magnetic moment than Gd^{3+} resulting from the interaction between the spin−orbital moment L and the electronic spin moment S leading to the spin angular moment J ($J = L + S$) was used. In this case, the χT value is equal to 10.95 $cm^3.K.mol^{-1}$ (**3**), but very low relaxivity values equal to 0.11 and 2.7 mM^{-1} s^{-1} for r_1 and r_2, respectively, were observed (Table 2, Figure S13c).

These qualitative investigations on the relaxivities obtained in the series of $Ln^{3+}/[M'(CN)_6]^{3-}$@Stabilizer nanoparticles (Ln = Gd, Tb, Y; M′ = Fe, Co) point out the complex role of several parameters and an absence of a direct correlation between the magnetic moment of the nanoparticles and their relaxivity. We have shown that the presence of Gd^{3+} ions in the structure with high electronic spin without spin−orbit coupling is crucial to maintain high values of r_1. In addition, the presence of another paramagnetic ion covalently linked to Gd^{3+} and obviously the presence of magnetic Gd^{3+}−Fe^{3+} interactions through cyanide bridges seems to be important. The complex combination of all mentioned factors offers longitudinal relaxivity value in the range 10−13 mM^{-1} s^{-1}, which is four times higher than the values of commercial CAs. Note that the stability of the nanoparticles will be further investigated in order to exclude the possibility of a partial Gd^{3+} release.

Let us now analyze the relaxivity behavior of nanosized Prussian blue and its anaologous nanoparticles. As previously mentioned, they present a face-centered cubic crystal structure (Figure S2) different from that of the compounds $Ln(H_2O)_4[Fe(CN)_6]$, while also having two different types of water molecules: coordinated water molecules completing the coordination sphere of the divalent transition metals arising from cyanometallate vacancies and crystallized water. In that case, both inner-sphere T_1- and outer-sphere T_2- relaxation mechanisms may also be operational for the relaxivity.[19,20] However, due to the nonstoichiometry of this family of compounds, several coordination environments around the divalent ion $[M(NC)_{6-x}(OH_2)_x]$ are observed and have recently been revealed spectroscopically by solid-state NMR.[35] Logically, it is expected that the nanoparticles of Prussian blue[19−23] exhibit lower values of r_1 compared to those obtained for the gadolinium-based nanoparticles, due to a smaller spin value of the paramagnetic centers with coordinated water molecules as well as the reduced number of such sites. However, the relaxivity of Prussian blue analogues was never investigated except recently published results on $Mn_2[Fe(CN)_6]$ nanoparticles showing extremely high values of r_2 = 117 mM^{-1} s^{-1} at 7 T (r_1 = 6.07 mM^{-1} s^{-1}).[22] Indeed, for nanoparticles of Prussian blue **7**, the obtained modest r_1 and r_2 values of 0.103 ± 0.001 mM^{-1} s^{-1} and 0.738 ± 0.008 mM^{-1} s^{-1} at 7 T or 0.095 ± 0.01 mM^{-1} s^{-1} and 2.05 ± 0.03 mM^{-1} s^{-1} at 4.7 T (Figures S14 and S15), respectively, are close to the previously reported values for Prussian Blue nanoparticles of 13 ± 5 nm capped with citrate (i.e., r_1 = 0.14 s^{-1} mM^{-1} or 0.079 mM^{-1} s^{-1}).[19,20] In this study, we have evaluated the relaxivity values for two Prussian blue analogues containing divalent metal ion Ni^{2+} (S = 1), i.e., $Ni^{2+}/[Fe(CN)_6]^{3-}$@PEG1000 nanoparticles **5** of 2.95 nm, and Cu^{2+} ($S = 1/2$), i.e., $Cu^{2+}/[Fe(CN)_6]^{3-}$@PEG1000 **6** of 5.52 nm. The ^1H NMR relaxometry characterizations (i.e., NMR-Dispersion profile) of **5** and **6** were performed at room temperature by measuring the longitudinal and transverse nuclear relaxation times, T_1 and T_2, of the solvent in the frequency range 10 kHz ≤ ν ≤ 212 MHz for T_1 and 15 MHz ≤ ν ≤ 60 MHz for T_2. The frequency dependence of r_1 and r_2 relaxivities for samples **5** and **6** as well as for the commercial CA Endorem (or Ferumoxide) are shown in Figure S14. In both cases, r_1 and r_2 values are much lower than those obtained for Endorem and do not seem to be frequency dependent. For comparison, at 60 MHz they are equal to 0.08 and 1.32 $mM^{-1}.s^{-1}$ for **5** and 0.26 and 1.09 mM^{-1} s^{-1} for **6**. In addition to the lower spin value compared to gadolinium, these moderate relaxivity values can originate also from the slower water exchange rate constant. Indeed, this constant is of the order 10^5 s^{-1} for the Ni^{2+} ion, a thousand times slower than the typical value for a gadolinium.

3. CONCLUSION

In summary, the concept of using cyano-bridged coordination polymer nanoparticles stabilized in aqueous solution by biocompatible stabilizing agents appears to be a promising route to provide new MRI CAs with improved relaxivity properties. In this article, we prepared a series of cyano-bridged coordination nanoparticles $Ln^{3+}/[M(CN)_6]^{3-}$/Stabilizer (where $Ln^{3+} = Gd^{3+}$, Y^{3+}, Tb^{3+}; $M = Fe^{3+}$, Co^{3+}) and nanosized Prussian blue and its analogues $M^{2+}/[Fe(CN)_6]^{3-}$/Stabilizer (M = Ni, Cu, Fe) with Stabilizer = polyethylene glycols (MW = 400 or 1000), polyethylene glycol functionalized with amine groups (MW = 1500) or by the sugar derivative N-acetyl-D-glucosamine. In all cases we obtained spherical nanoparticles uniform in size and shape, nonaggregated and well-dispersed in water with an average size 2−3.4 nm. The size and the shape of these nanoparticles are not significantly influenced by the nature and the coordinative function of the stabilizing agents employed. The longitudinal, T_1, and transverse, T_2, relaxation times are linearly dependent on the concentration of all nanoparticles allowing us to determine their longitudinal, r_1, and transverse, r_2, relaxivities (per paramagnetic ions) at room temperature under an applied magnetic field of 4.7 and 7 T. The relaxometry measurements as a function of frequency were also conducted for representative examples of each type of nanoparticles (Ln-containing or Prussian blue type).

Although the complete understanding of the relaxometry mechanism remains a complex process, we studied the influence of various parameters such as the spin value of lanthanide and transition metal ions, their anisotropy, the magnetic moments of the nanoparticles, and the nature of the stabilizing agent on the relaxivity. We showed that the nature and coordination of the stabilizing agent does not influence the relaxivity properties, while the electronic spins of lanthanide and transition metal ions and their magnetic properties as well as a crystal structure of the cyano-bridged network strongly impact the relaxivity. Indeed, for the $Gd^{3+}/[Fe(CN)_6]^{3-}$ nanoparticles of 2−3 nm, the Gd^{3+} ion possesses two coordinated and two crystallized water molecules which can be efficiently exchanged. The size of nanoparticles appears appropriate providing the location of most of the paramagnetic centers at the surface and a possible fast diffusion of water molecules at the core which offers an easy access path to the water molecule exchange. On the other hand, a larger size of the nanoparticles compared to the mononuclear Gd^{3+} complexes provides a decrease of the molecular tumbling and thus an increase in relaxivity. The complex combination of these factors offers longitudinal relaxivity value up to 12.6 $mM^{-1}\ s^{-1}$, which is four times higher than the values of commercial CAs. As for the molecular complexes, the presence of the Gd^{3+} ion with a high electronic spin, a low longitudinal electronic-spin relaxation rate, and high water exchange rate constant seems essential for high relaxivity. The latter vanishes completely if another lanthanide ion, even if this is paramagnetic with a high magnetic moment such as Tb^{3+}, is used instead of Gd^{3+}. The presence of a second paramagnetic transition metal ion covalently linked to Gd^{3+} via cyanide bridges of the coordination polymer network also appears to be an important parameter, which increases twice the relaxivity value relative to the use of a diamagnetic ion. Thus, even if the magnetic exchange between Gd^{3+} and Fe^{3+} through cyanide bridges is not observed by the macroscopic technique magnetometry at room temperature, it strongly influences the relaxivity properties. Finally, using the room temperature χT values of the nanoparticles and comparing them with the relaxivity, we also demonstrated that no direct dependence between these parameters may be observed for our nanoparticles. Most probably, this effect is due to some mechanisms compensating the increase of effective magnetic moment (χT value) that should lead anyway to the increase of relaxivity. As compared to nanoparticles $Gd^{3+}/[Fe(CN)_6]^{3-}$, nanosized Prussian blue and its analogues $M^{2+}/[Fe(CN)_6]^{3-}$ (M = Ni, Cu, Fe) have moderate relaxivity values which may be explained by the low electronic spins of transition metal ions and their relatively low exchange rate.

Thus, in this manuscript we described and compared the relaxivity properties of cyano-bridged coordination polymer nanoparticles of different compositions. The r_1 relaxivity values obtained for $Gd^{3+}/[Fe(CN)_6]^{3-}$ nanoparticles were proven to be at least four times higher (r_1 = 10−16 $mM^{-1}\ s^{-1}$) than those of gadolinium-based mononuclear commercial CAs and can be regarded as T_1-relaxing CAs of potential interest.

EXPERIMENTAL SECTION

Syntheses. Unless otherwise noted, all manipulations were performed at ambient temperature using reagents and solvents as received.

Synthesis of $Ln^{3+}/[M(CN)_6]^{3-}$@Stabilizer. An aqueous solution of $K_3[M(CN)_6]$ (0.2 mmol, 5 mL, M = Fe, Co) containing the appropriate amount of stabilizer (NADG: 0.05 mmol, $PEGNH_2$ = 0.05 mmol, PEG400 = 1.25 mmol, PEG1000 =1 mmol) was mixed with a $Ln(NO_3)_3{\cdot}nH_2O$ (n = 5 or 6) solution containing the same amount of stabilizer. The mixture is stirred for 2 h for PEG-NH_2 and NADG stabilizers and 18 h for PEG400 before being centrifugated 10 min at 20 000 rpm to remove any precipitate that may form. The supernatant is then filtered on a 0.45 μm filter and the obtained nanoparticles were precipitated with acetone and washed. The aqueous solutions for relaxometry measurements have been prepared from precipitated nanoparticles with addition of few drops of the corresponding stabilizer.

$Gd^{3+}/[Fe(CN)_6]^{3-}$@PEG400 (1a). $\nu_{-OH\ (H2O\ coordinated)}$ = 3614 cm^{-1}, $\nu_{-OH\ (H2O\ noncoordinated)}$ = 3420 cm^{-1} and 3265 cm^{-1}, ν_{C-H} = 2975 cm^{-1}, 2929 cm^{-1}, $\nu_{C\equiv N}$ = 2150 cm^{-1}, 2140 cm^{-1}, 2108 cm^{-1}, 2097 cm^{-1}, 2066 cm^{-1}, $\delta_{H-O-H\ coordinated}$ = 1678 cm^{-1}, 1635 cm^{-1}, 1608 cm^{-1}. El. anal., wt %: Gd, 34.28; Fe, 12.13; N, 18.17; C, 25.31; H, 1.97; O, 6.93. Determined from elemental analysis formula: $Gd[Fe(CN)_6]@(PEG400)_{0.21}$.

$Gd^{3+}/[Fe(CN)_6]^{3-}$@PEG1000 (1b). $\nu_{-OH\ (H2O\ coordinated)}$ = 3602 cm^{-1}, $\nu_{-OH\ (H2O\ noncoordinated)}$ = 3410 cm^{-1} and 3260 cm^{-1}, ν_{C-H} = 2970 cm^{-1}, 2930 cm^{-1}, $\nu_{C\equiv N}$ = 2070 cm^{-1}, 2140 cm^{-1}, 2150 cm^{-1}, $\delta_{H-O-H\ coordinated}$ = 1680 cm^{-1}, 1640 cm^{-1}, 1600 cm^{-1}. El. anal., wt %: Gd, 29.32; Fe, 10.84; N, 16.03; C, 28.98; H, 2.52; O, 10.79. Determined from elemental analysis formula: $Gd[Fe(CN)_6]@(PEG1000)_{0.16}$.

$Gd^{3+}/[Fe(CN)_6]^{3-}$@$PEGNH_2$ (1c). FTIR (KBr, ν cm^{-1}): $\nu_{-OH\ (H2O\ coordinated)}$ = 3614 cm^{-1}, $\nu_{-OH\ (H2O\ non\ coordinated)}$ = 3416 cm^{-1} and 3264 cm^{-1}, ν_{C-H} = 2960 cm^{-1}, 2929 cm^{-1}, $\nu_{C\equiv N}$ = 2150 cm^{-1}, 2140 cm^{-1}, 2108 cm^{-1}, 2066 cm^{-1}, $\delta_{H-O-H\ coordinated}$ = 1681 cm^{-1}, 1635 cm^{-1}, 1608 cm^{-1}. El. anal., wt %: Gd, 31.23; Fe, 10.56; N, 18.63; C, 28.93; H, 2.14; O, 10.22. Determined from elemental analysis formula: $Gd[Fe(CN)_6]@(PEGNH_2)_{0.10}$.

$Gd^{3+}/[Fe(CN)_6]^{3-}$@NADG (1d). FTIR (KBr, ν cm^{-1}): $\nu_{-OH\ (H2O\ coordinated)}$ = 3613 cm^{-1}, $\nu_{-OH\ (H2O\ non\ coordinated)}$ = 3423 cm^{-1} and 3264 cm^{-1}, ν_{C-H} = 2921 cm^{-1}, $\nu_{C\equiv N}$ = 2150 cm^{-1}, 2139 cm^{-1}, 2108 cm^{-1}, 2098 cm^{-1}, 2066 cm^{-1}, $\delta_{H-O-H\ coordinated}$ = 1680 cm^{-1}1, 1635 cm^{-1}, 1608 cm^{-1}. El. anal., wt %: Gd, 34.01; Fe, 10.93; N, 18.16; C, 24.32; H, 1.65; O, 9.77. Determined from elemental analysis formula: $Gd[Fe(CN)_6]@(NADG)_{0.48}$.

$Gd^{3+}/[Co(CN)_6]^{3-}$@PEG400 (2). FTIR (KBr, ν cm^{-1}): $\nu_{-OH\ (H2O\ coordinated)}$ = 3610 cm^{-1}, $\nu_{-OH\ (H2O\ non(coordinated)}$ = 3416 cm^{-1} and 3260 cm^{-1}, ν_{C-H} = 2923 cm^{-1}, 2850 cm^{-1}, $\nu_{C\equiv N}$ = 2162 cm^{-1}, 2139 cm^{-1}, 2154 cm^{-1}, 2120 cm^{-1}, 2111 cm^{-1}, $\delta_{H-O-H\ coordinated}$ = 1684 cm^{-1}, 1636 cm^{-1}, 1607 cm^{-1}. El. anal., wt %: Gd, 35.57; Co, 12.29; N, 18.18; C, 25.22; H, 1.87; O, 5.55. Determined from elemental analysis formula: $Gd[Co(CN)_6]@(PEG400)_{0.22}$.

dx.doi.org/10.1021/ic401710j | Inorg. Chem. 2013, 52, 13402−13414

$Tb^{3+}/[Fe(CN)_6]^{3-}$@PEG400 (3). FTIR (KBr, ν cm^{-1}): $\nu_{-OH\ (H2O\ coordinated)}$ = 3612 cm^{-1}, $\nu_{-OH\ (H2O\ noncoordinated)}$ = 3422 cm^{-1} and 3260 cm^{-1}, ν_{C-H} = 2974 cm^{-1}, $\nu_{C\equiv N}$ = 2150 cm^{-1}, 2140 cm^{-1}, 2109 cm^{-1}, 2098 cm^{-1}, 2066 cm^{-1}, $\delta_{H-O-H\ coordinated}$ = 1635 cm^{-1}, 1608 cm^{-1}. El. anal., wt %: Tb, 33.29; Fe, 11.23; N, 18.10; C, 25.32; H, 2.11; O, 7.57. Determined from elemental analysis formula: $Tb[Fe(CN)_6]@(PEG400)_{0.24}$.

$Y^{3+}/[Fe(CN)_6]^{3-}$@PEG400 (4). FTIR (KBr, ν cm^{-1}): $\nu_{-OH\ (H2O\ coordinated)}$ = 3613 cm^{-1}, $\nu_{-OH\ (H2O\ non\ coordinated)}$ = 3426 cm^{-1} and 3268 cm^{-1}, ν_{C-H} = 2921 cm^{-1}, 2848 cm^{-1}, $\nu_{C\equiv N}$ = 2122 cm^{-1}, 2143 cm^{-1}, 2111 cm^{-1}, 2099 cm^{-1}, 2069 cm^{-1}, $\delta_{H-O-H\ coordinated}$ = 1636 cm^{-1}, 1608 cm^{-1}. El. anal., wt %: Y, 23.31; Fe, 14.06; N, 21.39; C, 30.58; H, 2.42; O, 10.62. Determined from elemental analysis formula: $Y[Fe(CN)_6]@(PEG400)_{0.22}$.

Synthesis of $M^{2+}/[Fe(CN)_6]^{3-}$@PEG1000 (M = Ni, 5, Cu 6). Five mL of an aqueous $K_3[Fe(CN)_6]$ solution (2.8×10^{-2} M, 46.9 mg) containing 4.0×10^{-5} mol of PEG1000 was mixed with 5 mL of an aqueous $Ni(NO_3)_3{\cdot}6H_2O$ or $Cu(NO_3)_3{\cdot}6H_2O$ solution (3.2×10^{-2} M, 46.8 mg) containing 4.0×10^{-5} mol of stabilizer. After reaction, the solution is centrifuged 10 min at 20 000 rpm before being filtered (0.45 μm pore size). The obtained nanoparticles were precipitated with acetone and washed. The aqueous solutions for relaxometry measurements have been prepared from precipitated nanoparticles.

$Ni^{2+}/[Fe(CN)_6]^{3-}$@PEG1000 (5). FTIR (KBr, ν cm^{-1}): $\nu_{-OH\ (H2O\ coordinated)}$ = 3630 cm^{-1}, $\nu_{-OH\ (H2O\ noncoordinated)}$ = 3400 cm^{-1}, ν_{C-H} = 2920 cm^{-1} and 2880 cm^{-1}, $\nu_{C\equiv N}$ = 2167 cm^{-1} and 2119 cm^{-1}, $\delta_{H-O-H\ coordinated}$ = 1600 cm^{-1}, δ_{Fe-C-N} = 600 cm^{-1}. EDS Ni/Fe = 1.48.

$Cu^{2+}/[Fe(CN)_6]^{3-}$@PEG1000 (6). FTIR (KBr, ν cm^{-1}): $\nu_{-OH\ (H2O\ coordinated)}$ = 3625 cm^{-1}, $\nu_{-OH\ (H2O\ noncoordinated)}$ = 3405 cm^{-1}, ν_{C-H} = 2923 cm^{-1} and 2880 cm^{-1}, $\nu_{C\equiv N}$ = 2115 cm^{-1} and 2170 cm^{-1}, $\delta_{H-O-H\ coordinated}$ = 1600 cm^{-1}, δ_{Fe-C-N} = 600 cm^{-1}. EDS Cu/Fe = 1.45.

Synthesis of $Fe^{2+}/[Fe(CN)_6]^{3-}$@$PEGNH_2$ (7). 70 mL of an aqueous $K_3[Fe(CN)_6]$ solution (5.6×10^{-2} M, 1.29 g) containing 7.4×10^{-4} mol of $PEGNH_2$ was mixed with 70 mL of an aqueous $Fe(BF_4)_2{\cdot}6H_2O$ solution (4.2×10^{-2} M, 1.00 g) containing 4.0×10^{-5} mol of $PEGNH_2$. After stirring, the solution is centrifuged 10 min at 20 000 rpm before being filtered (0.45 μm pore size). The obtained nanoparticles were precipitated with acetone and washed. The aqueous solutions for relaxometry measurements have been prepared from precipitated nanoparticles.

FTIR (KBr, ν cm^{-1}): $\nu_{-OH\ (H2O\ noncoordinated)}$ = 3424 cm^{-1}, ν_{C-H} = 2960 cm^{-1}, 2912 cm^{-1}, 2875 cm^{-1}, $\nu_{C\equiv N}$ = 2075 cm^{-1}, $\delta_{H-O-H\ coordinated}$ = 1611 cm^{-1}.

Physical Measurements. Infrared spectra were recorded as KBr disks on a Perkin-Elmer 1600 spectrometer with a 4 cm^{-1} resolution. Elemental analyses were performed by the Service Central d'Analyses (CNRS, Vernaison, France). The samples were heated at 3000 °C under He. Oxygen was transformed in CO and detected by using an IR detector. Metals were determined with a high resolution ICP-MS using a ThermoFischer element. Magnetic susceptibility data were collected with a Quantum Design MPMS-XL SQUID magnetometer working in the temperature range 1.8−350 K and up to 7 T. Transmission Electron Microscopy (TEM) observations were carried out at 100 kV (JEOL 1200 EXII). Samples for TEM measurements were deposited from solutions on copper grids. The NPs size distribution histogram were determined using enlarged TEM micrographs taken at magnification of 100 K on a statistical sample of ca. 300 NPs. An evaluation of the M/M′ ratio was performed by using an Environmental Secondary Electron Microscope FEI Quanta 200 FEG coupled with an Electrons Dispersive Spectroscope Oxford INCA detector.

The ^{1}H NMR relaxometry characterizations have been performed by using aqueous solutions of **1**−**7** prepared from powder samples by their redispersion in water with few drops of corresponding stabilizing agent. The longitudinal (T_1) and transverse (T_2) relaxation time measurements for different concentrations of CAs were performed on a Tecmag Apollo spectrometer operating at 200 MHz. An inversion recovery sequence (180° − τ − 90°) was used to measure the longitudinal relaxation time T_1. τ was varied from a small value to a large value. For each concentration of the CA, the table of delay (τ) was chosen such that the instantaneous magnetization $M_z(t)$ recovers its equilibrium value M_0. Thereby, each T_1 value was obtained by curve fitting using the relation:

$$M_z(t) = M_0 \times [1 + (\cos\theta - 1) \times \exp(-t/T_1)] \quad (1)$$

where $M_z(t)$ represents the longitudinal magnetization at time t following the inversion pulse $\theta = \pi$. The Carr-Purcell Meiboom Gill pulse sequence $(90°-(180°)_n-)$ was applied to achieve the transverse relaxation time, T_2, measurement. These pulses are equidistantly spaced by an echo time t_e. For each concentration of CA, the number of echos (n) is selected to allow a complete decay of the transverse magnetization. The T_2 value was obtained by fitting the following relation:

$$M_{x,y}(nt_e) = M_0 \times \exp(-nt_e/T_2) \quad (2)$$

where $M_{x,y}(nt_e)$ is instantaneous transverse magnetization. The r_1 and r_2 relaxivities were then calculated from the slope of a linear regression of $R_{1,2} = T^{-1}{}_{1,2}$ against the concentration of the CA (C), following:

$$R_{1,2} = R^0{}_{1,2} + r_{1,2} \times C \quad (3)$$

where $R^0{}_{1,2}$ are the relaxation rates without CAs.

The ^{1}H NMR relaxometry characterization (i.e., NMR-Dispersion profile) of samples was performed at room temperature by measuring the longitudinal and the transverse nuclear relaxation times T_1 and T_2, in the frequency range 10 kHz $\leq \nu \leq$ 60 MHz for T_1 and 15 MHz $\leq \nu \leq$ 60 MHz for T_2. It should be noted that the measurements at room and physiological temperatures gave the same results within 10%. The efficiency of the MRI CAs is determined by measuring the nuclear relaxivities $r_{1,2}$ defined as:

$$r_i = [(1/T_i)_{meas} - (1/T_i)_{dia}]/c \qquad i = 1, 2 \quad (4)$$

where $(1/T_i)_{meas}$ is the value measured for the sample with concentration c (mmol L^{-1}) of magnetic center (4 mmol L^{-1} of Gd^{3+} for **1b**, 3.63 mmol.L^{-1} for **5**, and 1.13 mmol.L^{-1} for **6**) and $(1/T_i)_{dia}$ refers to the nuclear relaxation rate of the diamagnetic host solution (water in our case).

In vitro MRI acquisition experiments were performed on a 70/16 Pharmascan spectrometer (BRUKER Biospin, Ettlingen, Germany) equipped with a 7 Tesla magnet and 16-cm horizontal bore size, corresponding to a proton resonance frequency of 300 MHz. To acquire *in vitro* MR images and for T_1 and T_2 value measurements, CAs were dispersed in distilled water. The first phantom consisted of six 1.5-mL water vials with 0, 0.1, 0.5, 0.8, 1, 10 mmol L^{-1} concentrations of Gadoteridol (ProHance, Bracco Imaging, Italy) and the second phantom in six 1.5-mL water tubes with 0, 2, 5, 7.5, 10, 100-mmol L^{-1} concentrations of nanoparticles **7**. A linear birdcage coil with 38-mm inner diameter was used for signal transmission and reception. For **1a**, seven 1.5 mL water tubes with 0, 0.5, 1, 2, 5, 7.5, 10.6 mmol L^{-1} concentrations were placed in a linear birdcage coil with 62-mm inner diameter.

Both T_1- and T_2-weighted (T1W and T2W) axial images (slice thickness = 2 mm) were acquired using a turbo-RARE sequence (TE = 7.5 ms, TR = 700 ms, rare factor = 4, 2 averages for T1W and TE_{eff} = 60 ms, TR = 3000 ms, rare factor = 8, 2 averages for T2W) using a 256 × 256 matrix and a Field of View of 38-mm for Gadoteridol and nanoparticles **7** or 40-mm for **1a**. T_1 value measurements were performed using a multislice multiecho (MSME) sequence with TE = 4.5 ms and various TR: TR = 15, 50, 100, 500 ms (with 50 dummy scans), TR = 1000, 1500, 2000 ms (with 20 dummy scans), TR = 2500, 3000, 3500 ms (with 10 dummy scans), TR = 4000, 5000, 6000 ms (with 5 dummy scans), and TR = 8000, 10 000, 15 000, 20 000, 30 000 ms. T_2 value measurements were done with two MSME sequences with TE/TR = 4.5/12500 ms or TE/TR = 30/20000 ms, respectively, 1 average, and 256 echoes. The Field of View was 38-mm for Gadoteridol and **6** or 40-mm for **1a**, the matrix size was 64 × 64, and the slice thickness was 2 mm. In order to obtain the data processing for each tube, regions of interest (ROI) were surrounded on axial slices to determine the Signal to Noise Ratio (SNR). For T_1 and T_2 value determination, resulting curves were fitted with $I = I_0(1 - \exp(-TR/T_1))$ and $I = I_0.\exp(-TE/T_2))$, respectively. The r_1 and r_2 relaxivities were then calculated from the slope of a linear regression of longitudinal r_1 (=$1/T_1$) and transverse r_2

($=1/T_2$) relaxation rate, respectively, versus the concentration of the CAs.

■ ASSOCIATED CONTENT

Supporting Information

Additional information on structural description of Gd-$(H_2O)_4[Fe(CN)_6]$, PXRD pattern, TEM images, magnetic properties, relaxation rates measurements for samples **1**−**7**. This material is available free of charge via the Internet at http://pubs.acs.org.

■ AUTHOR INFORMATION

Corresponding Author

*Fax: (33) 4 67 14 38 52, e-mail: joulia.larionova@univ-montp2.fr.

Notes

The authors declare no competing financial interest.

■ ACKNOWLEDGMENTS

The authors thank Mme. C. Rebeil and Mme D. Granier (PAC Balard, Institute Charles Gerhardt Montpellier (ICGM), France) for magnetic and single crystal X-ray diffraction measurements. The authors also thank the ERA.NET-RUS project ST085 COPONAMRI, University of Montpellier and CNRS for funding. AL, MM and KVT thank the Italian FIRB RINAME project for partly supporting the research.

■ REFERENCES

(1) (a) Spokoyny, A. M.; Kim, D.; Sumrein, A.; Mirkin, C. A. *Chem. Soc. Rev.* **2009**, *38*, 1218. (b) Oh, M.; Mirkin, C. A. *Nature* **2005**, *438*, 651. (c) Horcajada, P.; Gref, R.; Baati, T.; Allan, P. K.; Maurin, G.; Couvreur, P.; Férey, G.; Morris, R. E.; Serre, Ch. *Chem. Rev.* **2012**, *112*, 1232.

(2) (a) Taylor, K. M. L.; Jin, A.; Lin, W. *Angew. Chem., Int. Ed.* **2008**, *47*, 7722. (b) Rocca, J. D.; Liu, D.; Lin, W. *Acc. Chem. Res.* **2011**, *44* (10), 957.

(3) (a) Vaucher, S.; Li, M.; Mann, S. *Angew. Chem., Int. Ed.* **2000**, *39*, 1793. (b) Catala, L.; Volatron, F.; Brinzei, D.; Mallah, T. *Inorg. Chem.* **2009**, *48*, 3360. (c) Larionova, J.; Guari, Y.; Sangregorio, C.; Guérin, Ch. *New J. Chem.* **2009**, *33*, 1177.

(4) (a) Férey, G.; Mellot-Draznieks, C.; Serre, C.; Millange, F.; Dutour, J.; Surblé, S. M.; Margiolaki, I. *Science* **2005**, *309*, 2040. (b) Férey, G.; Serre, C.; Mellot-Draznieks, C.; Millange, F.; Surblé, S. *Angew. Chem., Int. Ed.* **2004**, *116*, 6456. (c) Yang, B. B.; Abel, R. B.; Upruchard, A. C. G.; Smithers, J. A.; Forgue, S. T. *J. Clin. Pharmacol.* **1996**, *36*, 623. (d) Taylor-Pashow, K. M. L.; Della Rocca, J.; Xie, Z.; Tran, S.; Lin, W. *J. Am. Chem. Soc.* **2009**, *131*, 14261. (e) Ke, F.; Yuan, Y.-P.; Qiu, L.-G.; She, Y.-H.; Xie, A.-J.; Zhu, J.-F.; Tian, X.-Y.; Zhang, L.-D. *J. Mater. Chem.* **2011**, *21*, 3843. (f) Miller, S. R.; Heurtaux, D.; Baati, T.; Horcajada, P.; Grenèche, J.-M.; Serre, C. *Chem. Commun.* **2010**, *46*, 4525. (g) Roy, X.; Hui, J. K.-H.; Rabnawaz, M.; Lui, G.; McLachlan, M. J. *J. Am. Chem. Soc.* **2011**, *133*, 8420. (h) Férey, G.; Mellot-Draznieks, C.; Serre, C.; Millange, F.; Dutour, J.; Surblé, S. M.; Margiolaki, I. *Science* **2005**, *309*, 2040. (i) Férey, G.; Serre, C.; Mellot-Draznieks, C.; Millange, F.; Surblé, S. *Angew. Chem., Int. Ed.* **2004**, *116*, 6456. (j) Yang, B. B.; Abel, R. B.; Upruchard, A. C. G.; Smithers, J. A.; Forgue, S. T. *J. Clin. Pharmacol.* **1996**, *36*, 623. (k) Taylor-Pashow, K. M. L.; Della Rocca, J.; Xie, Z.; Tran, S.; Lin, W. *J. Am. Chem. Soc.* **2009**, *131*, 14261. (l) Ke, F.; Yuan, Y.-P.; Qiu, L.-G.; She, Y.-H.; Xie, A.-J.; Zhu, J.-F.; Tian, X.-Y.; Zhang, L.-D. *J. Mater. Chem.* **2011**, *21*, 3843. (m) Miller, S. R.; Heurtaux, D.; Baati, T.; Horcajada, P.; Grenèche, J.-M.; Serre, C. *Chem. Commun.* **2010**, *46*, 4525.

(5) (a) Perera, V. S.; Hao, J.; Gao, M.; Gough, M.; Zavalij, P. Y.; Flask, C.; Basilion, J. P.; Huang, S. D. *Inorg. Chem.* **2011**, *50*, 7910. (b) deKrafft, K. E.; Xie, Z.; Gao, G.; Tran, S.; Ma, L.; Zhou, O. Z.; Lin, W. *Angew. Chem., Int. Ed.* **2009**, *48*, 9901.

(6) (a) Rieter, W. J.; Taylor, K. M. L.; An, H.; Lin, W. *J. Am. Chem. Soc.* **2006**, *128*, 9024. (b) Ye, S.; Liu, Y.; Chen, S.; Liang, S.; McHale, R.; Ghasdian, N.; Lu, Y.; Wang, X. *Chem Commun.* **2011**, *47*, 6831.

(7) Fu, G.; Liu, W.; Feng, S.; Yue, X. *Chem. Commun.* **2012**, *48*, 11567−11569.

(8) *Magnetic Resonance in Medicine*, 3rd ed.; Rinck, P. A., Ed.; Blackwell: Oxford, 1993.

(9) Callaghan, P. T.; Clarke, C. J.; Forde, L. C. *Biophys. Chem.* **1994**, *50*, 225−235.

(10) (a) Laurent, S. in *NMR-MRI, μSR and Mossbauer Spectroscopies in Molecular Magnets*; Carretta, P., Lascialfari, A., Eds.; Springer-Verlag: Italia, 2007; p 71. (b) Lascialfari, A.; Corti, M. In *NMR-MRI, mSR and Mossbauer Spectroscopies in Molecular Magnets*; Carretta, P., Lascialfari, A., Eds.; Springer-Verlag: Italy, 2007; p 89.

(11) (a) Caravan, P.; Elison, J. J.; McMurry, T. J.; Lauffer, R. B. *Chem. Rev.* **1999**, *99*, 2293. (b) Aime, S.; Botta, M.; Fasano, M.; Geninatti Crich, S.; Terreno, E. *Coord. Chem. Rev.* **1999**, *185*−*186*, 321. (c) *The Chemistry of Contrast Agents in Medical Magnetic Resonance Imaging*; Merbach, A. E., Toth, E. Eds.; Wiley: New York, 2001.

(12) (a) Werner, E. J.; Datta, A.; Jocher, C. J.; Raymond, K. N. *Angew. Chem., Int. Ed.* **2008**, *47*, 8568. (b) Aime, S.; Castelli, D. D.; Crich, S. G.; Gianolio, E.; Terreno, E. *Acc. Chem. Res.* **2009**, *42*, 822.

(13) (a) Bridot, J. L.; Faure, A. C.; Laurent, S.; Riviere, C.; Billotey, C.; Hiba, B.; Janier, M.; Josserand, V.; Coll, J. L.; Vander Elst, L.; Muller, R.; Roux, S.; Perriat, P.; Tillement, O. *J. Am. Chem. Soc.* **2007**, *129*, 5076. (b) Evanics, F.; Diamente, P. R.; van Veggel, F. C. J. M.; Stanisz, G. J.; Prosser, R. S. *Chem. Mater.* **2006**, *18*, 2499. (c) Park, J. Y.; Baek, M. J.; Choi, E. S.; Woo, S.; Kim, J. H.; Kim, T. J.; Jung, J. C.; Chae, K. S.; Chang, Y.; Lee, G. H. *ACS Nano* **2009**, *3*, 3663. (d) Hifumi, H.; Yamaoka, S.; Tanimoto, A.; Akatsu, T.; Shindo, Y.; Honda, A.; Citterio, D.; Oka, K.; Kuribayashi, S.; Suzuki, K. *J. Mater. Chem.* **2009**, *19*, 6393. (e) Johnson, N. J. J.; Oakden, W.; Stanisz, G. J.; Prosser, R. S.; van Veggel, F. C. J. M. *Chem. Mater.* **2011**, *23*, 3714.

(14) (a) Rowe, M. D.; Chang, C.-C.; Thamm, D. H.; Kraft, S. L., Jr.; Harmon, J. F.; Vogt, A. P.; Sumerlin, B. S.; Boyes, S. G. *Langmuir* **2009**, *25*, 9487. (b) Rieter, W. J.; Pott, K. M.; Taylor, K. M. L.; Lin, W. *J. Am. Chem. Soc.* **2008**, *130*, 11854. (c) Nishiyabu, R.; Hashimoto, N.; Cho, T.; Watanabe, K.; Yasunaga, T.; Endo, A.; Kaneko, K.; Niidome, T.; Murata, M.; Adachi, C.; Katayama, Y.; Hashizume, M.; Kimizuka, N. *J. Am. Chem. Soc.* **2009**, *131*, 2151. (d) Nishiyabu, R.; Aime, C.; Gondo, R.; Noguchi, T.; Kimizuka, N. *Angew. Chem., Int. Ed.* **2009**, *48*, 9465.

(15) (a) Horcajada, P.; Chalati, T.; Serre, Ch.; Gillet, B.; Sebrie, C.; Baati, T.; Eubank, J. F.; Heurtaux, D.; Clayette, P.; Kreuz, Ch.; Chang, J.-S.; Hwang, Y. K.; Marsaud, V.; Bories, Ph.-N.; Cynober, L.; Gil, S.; Férey, G.; Couvreur, P.; Gref, R. *Nat. Mater.* **2010**, *9*, 172. (b) Horcajada, P.; Serre, Ch.; Maurin, G.; Ramsahye, N. A.; Balas, F.; Vallet-Regí, M.; Sebban, M.; Taulelle, F.; Férey, G. *J. Am. Chem. Soc.* **2008**, *130*, 6774. (c) McKinlay, A. C.; Morris, R. E.; Horcajada, P.; Ferey, G.; Gref, R.; Couvreur, P.; Serre, Ch. *Angew. Chem., Int. Ed.* **2010**, *49*, 6260.

(16) Taylor, K. M. L.; Rieter, W. J.; Lin, W. *J. Am. Chem. Soc.* **2008**, *130*, 14358.

(17) Pereira, G. A.; Peters, J. A.; Paz, F. A.; Rocha, J.; Geraldes, C. F. *Inorg. Chem.* **2010**, *49*, 2969.

(18) (a) Uemura, T.; Kitagawa, S. *J. Am. Chem. Soc.* **2003**, *125*, 7814. (b) Domingez-Vera, J. M.; Colacio, E. *Inorg. Chem.* **2003**, *42*, 6983. (c) Xu, S.; Qian, X.; Li, G. *Mater. Res. Bull.* **2008**, *43*, 135. (d) Lian, H.-Y.; Hu, M.; Liu, C.-H.; Yamauchi, Y.; Wu, K. C.-W *Chem. Commun.* **2012**, *48*, 5151.

(19) Shokouhimehr, M.; Soehnlen, E. S.; Khitrin, A.; Basu, S.; Huang, S. D. *Inorg. Chem. Commun.* **2010**, *13*, 58.

(20) Sholouhimehr, M.; Soehnlen, E. S.; Hao, H. H.; Griswold, M.; Flask, C.; Fan, X. D.; Basilion, J. P.; Basu, S.; Huang, S. P. D. *J. Mater. Chem.* **2010**, *20*, 5251.

(21) Huang, S. D.; Li, Y.; Shokouhimehr M. Patent No WO 2011/106309 A2, 2011.

(22) Huang, S. D.; Khitrin, A. K.; Perera, V. S. Patent No WO 2012/108856 A1, 2012.

(23) Huang, S. D., Li, Y., Shokouhimehr, M. U. S. Patent US20090384391 20090403, 2010.

(24) Guari, Y.; Larionova, J.; Corti, M.; Lascialfari, A.; Marinone, M.; Poletti, G.; Molvinger, K.; Guérin, Ch. *Dalton Trans.* **2008**, 3658.
(25) Chelebaeva, E.; Larionova, J.; Guari, Y.; Ferreira, R. A. S.; Carlos, L. D.; Trifonov, A. A.; Kalaivani, T.; Lascialfari, A.; Guérin, Ch.; Molvinger, K.; Datas, L.; Maynadier, M.; Gary-Bobo, M.; Garcia, M. *Nanoscale* **2011**, *3*, 1200.
(26) Zhou, X.; Wong, W.-T.; Faucher, M. D.; Tanner, P. A. *J. Solid State Chem.* **2008**, *181*, 3057.
(27) (a) Reguera, E.; Bertran, J. F.; Diaz, C.; Blanco, J.; Rondon, S. *Hyperfine Interact.* **1990**, *53*, 391. (b) Buchold, D. H. M.; Feldmann, C. *Chem. Mater.* **2007**, *19*, 3376.
(28) Kulesza, P. J.; Malik, M. A.; Denca, A.; Strojek, J. *Anal. Chem.* **1996**, *68*, 2442.
(29) Cotton, S. *Lanthanide and Actinide Chemisty*; John Wiley and Sons, Ltd., 2006.
(30) Juszczky, S.; Johansson, C.; Hanson, M.; Ratuszna, A.; Malecki, G. *J. Phys.: Condens. Matter* **1994**, *6*, 5697.
(31) Ohkoshi, S.-I.; Nakagawa, K.; Tomono, K.; Imoto, K.; Tsunobuchi, Y.; Tokoro, H. *J. Am. Chem. Soc.* **2010**, *132*, 6620.
(32) Toth, E.; Helm, L.; Merbach, A. E. *Top. Curr. Chem.* **2002**, *221*, 61.
(33) Ferrante, G.; Sykora, S. *Adv. Inorg. Chem.* **2005**, *57*, 405.
(34) Caravan, P. *Chem. Soc. Rev.* **2006**, *35*, 512.
(35) Flambard, A.; Köhler, F. H.; Lescouëzec, R.; Caravan, P.; Ellison, J. J.; McMurry, T. J.; Lauffer, R. B. *Angew. Chem., Int. Ed.* **2009**, *48*, 1673.